J Mater Sci (2015) 50:1323–1332
DOI 10.1007/s10853-014-8692-3

Au nanoparticle decorated N-containing polymer spheres: additive-free synthesis and remarkable catalytic behavior for reduction of 4-nitrophenol

Shoupei Wang · Jianan Zhang · Pengfei Yuan · Qiang Sun · Yu Jia · Wenfu Yan · Zhimin Chen · Qun Xu

Received: 4 August 2014 / Accepted: 29 October 2014 / Published online: 7 November 2014

Abstract We demonstrated a simple, one-step route for assembling Au nanoparticles (NPs) on N-containing polymer nanospheres through in situ reductive growth process.Using resorcinol–melamine–formaldehyde resin nanospheres (RMF NSs) as a functional platform, neither a surfactant/ligand nor pretreatment is needed in the synthetic process of Au@RMF NSs hybrid nanostructure. When used as a catalytic media for the reduction of 4-nitrophenol (4-NP) to 4-aminophenol, the Au@RMF NSs hybrid nanostructures show significantly enhanced catalytic performance than the ever reported Au-based catalyst. The absorption modal of 4-NP on this nanostructure is also discussed by theoretical calculations using density functional theory. The calculated results verify the preferential capture of 4-NP by the N-containing functionalities of RMF NSs, which is critical step for the acceleration of Au-based catalytic reaction kinetics, leading to the remarkable improved catalytic behavior. The superior features of RMF NSs as well as minimal economical cost compared with other polymer and non-polymer will promote further interest in the field of N-containing catalysis.

Electronic supplementary material The online version of this article (doi:10.1007/s10853-014-8692-3) contains supplementary material, which is available to authorized users.

S. Wang · J. Zhang (✉) · Z. Chen · Q. Xu (✉)
College of Material Science and Engineering, Zhengzhou University, Zhengzhou 450001, People's Republic of China
e-mail: zjn@zzu.edu.cn

Q. Xu
e-mail: qunxu@zzu.edu.cn

P. Yuan · Q. Sun · Y. Jia
Physical Engineering College of Zhengzhou University, Zhengzhou University, Zhengzhou 450001, People's Republic of China

W. Yan
State Key Laboratory of Inorganic Synthesis and Preparative Chemistry, College of Chemistry, Jilin University, Changchun 130012, People's Republic of China

Introduction

The reductive conversion of nitroarenes has been attracting considerable attention, due to the increasing problems of environmental pollution caused by industrial products and agricultural waste [1]. As a commonly studied model, 4-aminophenol (4-AP) is an important intermediate for the manufacture of analgesic and antipyretic drugs and they can be synthesized by the catalytic hydrogenation of 4-nitrophenol (4-NP) [2, 3]. Gold is well established to be a high desirable catalyst toward reduction of 4-NP reaction [4–6]. To facilitate cyclic utilization of catalyst, Au NPs are frequently attached on/in various solid supports, such as polymer [7–9], metal oxide [10–12], carbon materials [13, 14], and natural materials [15], fabricating hybrid nanostructural catalysts. Among them, polymer is one of the most popular supports. The advantages of using polymer as support are not only the enhancement of long-term stability by stabilizing NPs, but also the tunable functionalization of Au NPs with polymer to achieve tailor properties of Au NPs [16–18]. Wang and co-workers have reported the synthesis of Au NPs immobilized on polyacrylonitrile fiber as catalyst for reduction of 4-NP reaction [19]. Fu and co-workers have stabilized Au NPs on the surfaces of polyphosphazenes/CNTs nanocables as high temperature toleration catalyst toward reduction of 4-NP reaction [20]. Lu and co-workers have reported the thermosensitive Au-polymer core–shell nanoparticles (NPs) for catalyzing reduction of 4-NP [21]. Despite these great efforts, the existing Au-polymer catalysts

still suffer from the unsatisfying activity and stability, owing to the lack of synergetic effects between the substrates and Au NPs toward the catalytic mechanism, which frequently exist in Au/inorganic supports, such as Au/TiO_2 and Au/CeO_2 [10, 22]. And this drawback has become the main obstacle to their commercialization. Therefore, the rational design and synthesis of more robust and practical Au-polymer with high activity and long-term reusability have been highly desired.

Recent studies have revealed that metal loaded on N-containing carbon [23, 24] and even N-doped graphene [25, 26] demonstrate remarkable enhanced performance for heterogeneous catalysis, electrochemistry, and supercapacitor. In the field of catalysis, the electron-riched N-containing groups have been found to be capable of providing both strong metal-support interactions for stabilizing NPs and smart active sites for binding or adsorption of organic molecules, which probably favor high catalytic activity and stability [27]. Prominent examples include the Pd/N-magnetic carbon NPs efficiently catalyzing Heck, Suzuki, and Sonogashira coupling reactions [27], Au/N-doped graphene for high selective oxidation of benzylic alcohols [28], and so forth. The fantastic effect of nitrogen-doped support on catalysis inspires us to evaluate whether such route can associated with the design of Au-loaded N-containing polymer hybrid catalyst with high performance, which will be of great interest and significance for the development of new hybrid catalyst.

In this paper, we demonstrated a convenient and cost-effective synthetic route for the preparation of Au NPs on N-containing polymer (RMF NSs) through in situ reductive growth process without any additive modification. Significantly, Au@RMF NSs hybrid nanostructure exhibited an excellent catalytic activity with k_{app} of 33×10^{-3} s^{-1} toward reduction of 4-NP reaction and good cycling life, which was remarkably better than that of the traditional Au-based catalysis, such as Au@SiO_2 NSs and Au@active carbon hybrid catalyst. More importantly, an optimized adsorption model was proposed by theoretical calculations using density functional theory (DFT), demonstrating that the N-containing functional groups existing in RMF NSs had significant role on the enhancement of reduction of 4-NP catalytic performance. Our work provides a new concept for enhancing the stability and activity by optimizing the structure of the catalyst.

Experimental

Preparation of the RMF NSs

In a typical synthesis of RMF resins NSs, 0.74 mL of formaldehyde (F) (37 %) and 0.55 g resorcinol (R) were dissolved in a mixture containing 0.5 mL of ammonia aqueous solution, 40 mL of ethanol, and 100 mL of distilled water at 70 °C under vigorous agitation. After stirring for 30 min, 550 mL of formaldehyde (37 %) and 0.315 g melamine (M) were added to the above mixture. The solution was kept stirring at 70 °C for 24 h and subsequently heated for 24 h at 100 °C in a Teflon-lined autoclave. The reddish brown powder (RMF resins NSs) was collected by centrifugation and washed with ethanol and water, followed by drying at 80 °C for 24 h in air.

Preparation of Au@RMF NSs hybrid structures

Au@RMF NSs hybrid structures were synthesized via an in situ reduction method as follows: 0.3 mL of 20 mM $HAuCl_4$ was dropwise added to RMF resins NSs aqueous dispersion (40 mL, 0.5 mg mL^{-1}). After 30 min, 0.7 mL of blending aqueous solution containing 50 mM sodium citrate and 0.01 % $NaBH_4$ were rapidly added to the above mixture. The product was collected by centrifugation and washed with water and ethanol, followed by drying at 80 °C overnight. As a comparison, the Au@SiO_2 NSs and Au@active carbon hybrid materials were also obtained by NH_2-group-modified SiO_2 NSs [29] (synthesized by stöber method) and active carbon via the above method.

Characterizations

Transmission electron microscopy (TEM) images were collected on a Tecnai G2 20 with an accelerating voltage of 200 kV. Scanning electron microscopy (SEM) images were taken by a field-emission scanning electron microscope (JEOL 7500) operating at 5 kV. X-ray diffraction (XRD) pattern of the product was recorded on a Rigaku D/MAX-3B using Cu Kα radiation (λ = 1.5406 Å). The Fourier transform infrared spectra were recorded from 400 to 4000 cm^{-1} on a Perkin-Elmer Paragon 1000 Fourier transform spectrometer using KBr pellets. The X-ray photoelectron spectroscopy (XPS) experiments were performed with an ESCA LAB 250 spectrometer using a focused monochromatic Al Kα (hv = 1486.6 eV) X-ray beam with a diameter of 200 μm. Element analyses (C, H, and N) were carried out with a Perkin-Elmer 2400 elemental analyzer. Thermogravimetric analysis (TGA) of the samples was monitored using a Mettler Toledo TGA/DSC 1 analyzer from 30 to 900 °C under air with a heating rate of 10 °C/min. UV–vis spectrum was performed on Shimadzu UV-240 spectrometer ranging from 250 to 450 nm. Dynamic light scattering was measured out at 25 °C on a Malvern Zetasizer NanoZS90 Instrument. Inductively coupled plasma mass spectrometry (ICP-MS) data were collected on an Aglient 7500a ICP-MS spectrometer.

Catalytic reaction

Typically, an aqueous 4-NP solution (1.7 mL, 2.0×10^{-4} mol L^{-1}) was mixed with aqueous solution of $NaBH_4$ (1.0 mL, 1.5×10^{-2} mol L^{-1}) in a cuvette (1 cm path length), resulting in a color change from light yellow to yellow green. Then, 0.1 mg of the catalysts was added to the mixture and quickly placed in the cell holder of spectrophotometer. The progress of the conversion of 4-NP to 4-AP was then monitored via UV–vis spectroscopy by recording the time-dependent absorbance spectra of the reaction mixture in a scanning range of 250-450 nm at ambient temperature. For catalytic reduction of 4-NP, 17 mL of 2.0×10^{-4} mol L^{-1} 4-NP solution was mixed with 10 mL of 1.5×10^{-2} mol L^{-1} $NaBH_4$ solution. Then, 0.2 mL (1 mg mL^{-1}) of the catalyst was injected rapidly. At the end of the reaction, the catalyst was separated from mixed solution through centrifugalization, followed by beginning the next cycle.

Computational simulations

All calculations were carried out using the DFT implemented in the Dmol3 code [30]. For the electronic structure calculation, all electron treatments and double numerical basis including d-polarization functions were chosen. The exchange–correlation interaction was treated within the generalized gradient approximation with the correction of the Perdew–Wang 1991 version [31]. In the geometry optimization, all atoms were allowed to relax without any symmetry restriction. The change of total energy, total forces on all atomic sites, and the displacement were less than 2.0×10^{-5} Ha, 0.004 Ha/A, and 0.005 A, respectively. The adsorption energy was calculated as follows: $E_{ads} = E_{system} - E_{composite} - E_{4\text{-NP}}$, where E_{system}, $E_{composite}$, and $E_{4\text{-NP}}$ were the total energies of free 4-NP ion on RMF dimer, RMF dimer, and the isolated 4-NP ion, respectively. A more negative E_{ads} demonstrated a more stable interaction between 4-NP ion and composite.

Results and discussion

The representative synthetic procedures for RMF NSs and Au@RMF NSs are illustrated in Scheme 1. RMF NSs were obtained by co-condensation of resorcinol–formaldehyde precursor and melamine–formaldehyde resins precursor in the water–ethanol–ammonium system (Scheme 1a) [32–34]. Figure 1 shows the typical SEM and TEM images of the as-prepared RMF NSs. The RMF NSs with smooth surfaces have the uniform diameter of 250–300 nm and good dispersibility. During the synthetic process of RMF NSs, we found that by increasing the initial mole ratio of R:M, the surface bonding and tension decreased, smaller sized clusters were formed at initial stage, which led to smaller-size RMF resins colloid nanospheres (Fig. S1). Then, the Au NPs could be in situ loaded on the surfaces of RMF NSs by reducing the $AuCl_4^-$ precursor adsorbed around the RMF NSs (Scheme 1b). The triazine- and amino-groups of RMF NSs may act as ligands to stabilize the Au NPs. The formation of the 3-D RMF networks in the nanospheres was demonstrated by FT-IR and XPS measurements (Fig. 2). Figure 2a shows the comparison for FI-IR spectra of RF NSs (line a), RMF NSs (line b), and pure melamine (line c). The three individual absorption bands at 1610, 1349, and 811 cm^{-1} in the spectra of RMF NSs and pure melamine are attributed to the aromatic C–N stretching and "breathing" modes in the triazine unit, respectively, while these peaks are not observed in RF NSs [24]. The XPS spectra of RMF NSs (shown in Fig. 2b–d) can further verify the formation of co-condensation in the RMF system. The N1s spectra could be deconvoluted into two peaks with binding energies of 398.4 and 399.6 eV, corresponding to the neutral nitrogen atoms (C–NH–C) and triazine nitrogen atoms (C=N–C), respectively [35]. The relative intensities of these two peaks are similar, which can only come from melamine. No peak associated with nitrogen bonded to oxygen was observed, suggesting that the oxygen atoms might be bonded to the carbon atoms [36]. It was also found that the C 1s peaks could be fitted to three shapes with binding energies at 287.8, 285.04, and 284.4 eV, assigned to the C atoms in the triazine ring (N=C–N), C–N or C–O and C–C, respectively [37]. Based on the above results, we can prove the formation of the 3-D RMF networks by our synthetic method. The contents of N in RMF NSs were determined to be 7.96 % (monitored by CHN element analysis), being in good agreement with the XPS results.

Figure 3a and b shows the TEM images of as-prepared Au@RMF NSs at different magnifications. We could see that almost all the Au NPs are nicely dispersed on the surfaces of RMF NSs. In order to reveal the detailed structure of Au@RMF NSs, their corresponding magnified TEM image is shown in Fig. 3b. The Au NPs with the size distribution of 2–6 nm, the average size of which is ca. 3.5 nm, (Fig. 3c) were supported on the surfaces of RMF NSs with uniform dispersion. Such size of Au NPs has been suggested as an optimal diameter for catalytic applications [38]. The wide-angle XRD patterns and XPS spectrum of Au@RMF hybrid nanostructures are given in Fig. 3d and S2. The wide diffraction peaks at 38.21°, 44.41°, 64.51°, and 77.61° are assigned to the (111), (200), (220), and (311) crystal planes of face-centered cubic gold, respectively. In addition, it is noteworthy that no other reflections are observed in the XRD pattern, demonstrating that no significant quantities of precursors remain in the

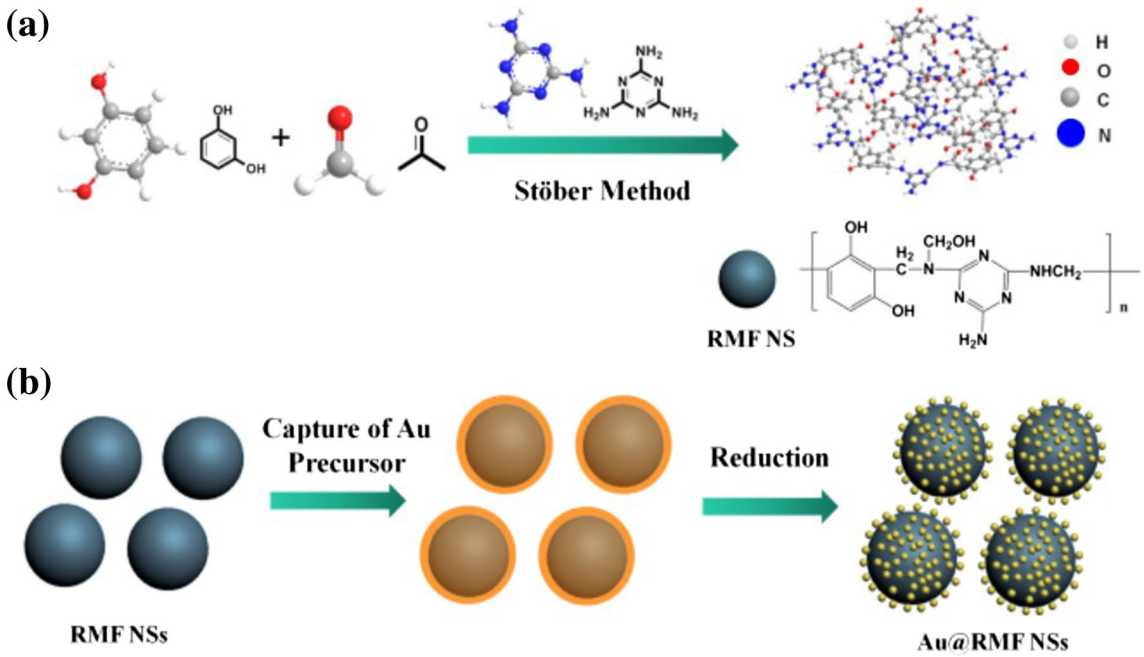

Scheme 1 Illustration of the procedure for preparing the **a** RMF NSs and **b** Au@RMF NSs catalyst

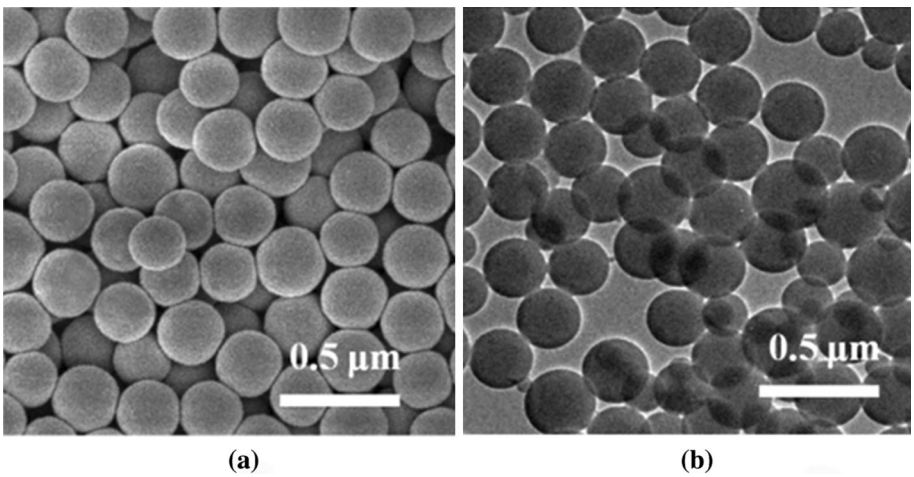

Fig. 1 **a** SEM image and **b** TEM image of RMF NSs

RMF NSs matrix [39]. The XRD data are consistent with the result of TEM characterization. As shown in Fig. S2, the bonding energies at 84.1 and 87.8 eV are associated with the Au $4f_{7/2}$ and Au $4f_{5/2}$ of Au^0, respectively, indicating the completely reduction of Au NPs [40]. The content of Au NPs on the MRF resins NSs is about 4.0 %, monitored by ICP-MS.

As a comparison experiment, we also synthesized RF NSs as a supporter (Fig. S3), the TEM shows only a few of Au NPs were loaded on RF NSs, indicating that the triazine- and amino-group of melamine probably play an important role in stabilizing Au NSs. The strong interaction occurred between Au NPs and RMF NSs was further demonstrated by FI-IR spectroscopy. As shown in Fig. 4a, after the Au NPs were immobilized onto the surfaces of the RMF resin NSs, a spectral peak shift of 49 cm^{-1} for C=N bond in the triazine unit band from 1349 to 1398 cm^{-1} and a same blue peak shift for N–H bond in the amino-group from around 3342 to 3391 cm^{-1} were obviously observed. The blue shift of the C=N and N–H bonds implies that strong ligand bond form between RMF NSs and Au NPs. The strong interaction will be benefit for the catalytic stability of Au NPs.

The thermo behavior Au@RMF NSs were also detected by the TGA measurement (Fig. 4b) performed over the range of temperature 30–800 °C under a flowing air atmosphere at a heating rate of 5 °C/min. The TGA of pure RMF resin NSs was also added for comparison. It should

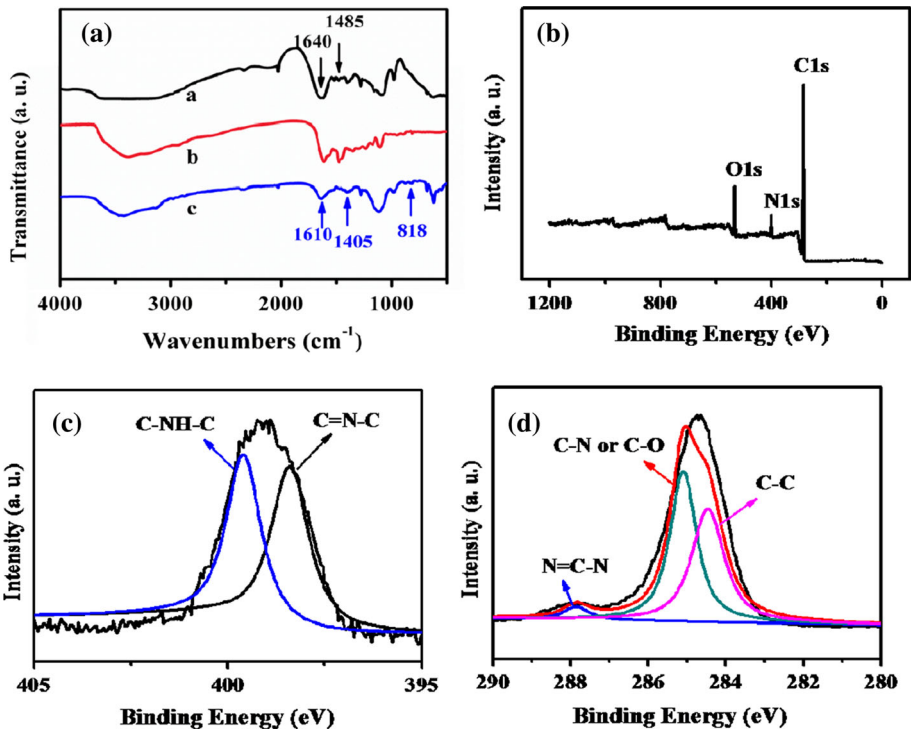

Fig. 2 **a** FI-IR spectra of RF NSs (*line a*), RMF NSs (*line b*), and pure melamine (*line c*). XPS spectra of RMF resins NSs: **b** survey, **c** N1s and **d** C1s

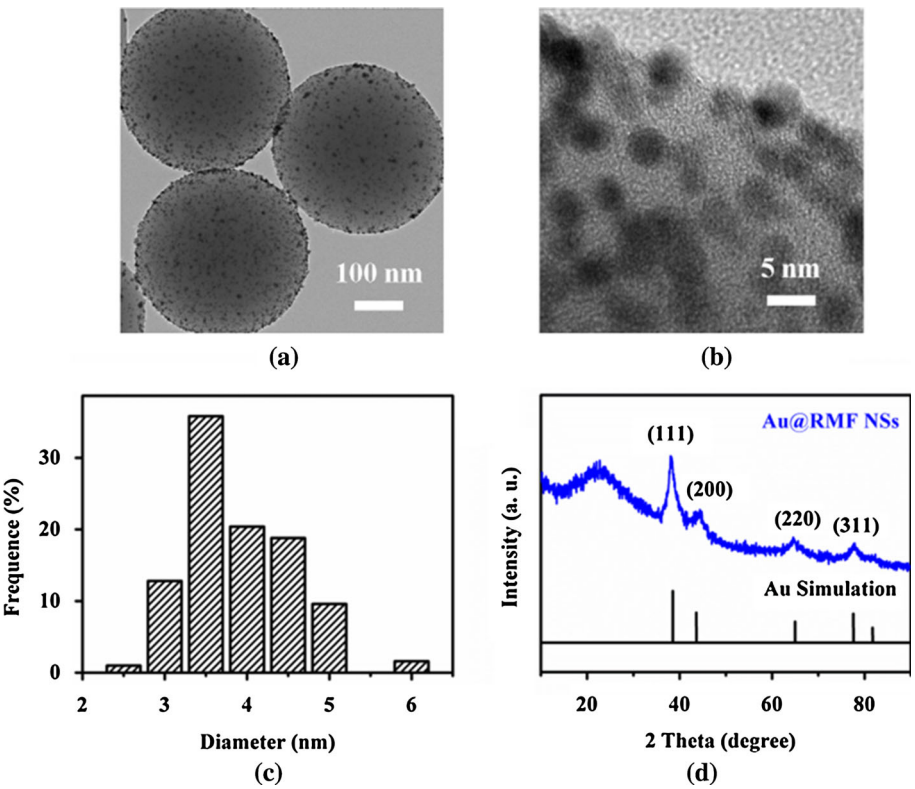

Fig. 3 **a** TEM and **b** HR-TEM images of Au@RMF NSs. **c** The size distribution of Au NPs. **d** XRD patterns of Au@RMF NSs and Au simulation

be noted that the initial weight loss of the Au@RMF NPs composites at about 30–100 °C should be assigned to the elimination of the adsorbed water. The decomposition of the RMF NSs started at approximately 235 °C and the loaded Au NPs do not significantly affect the initial decomposition temperature of the polymer, and the

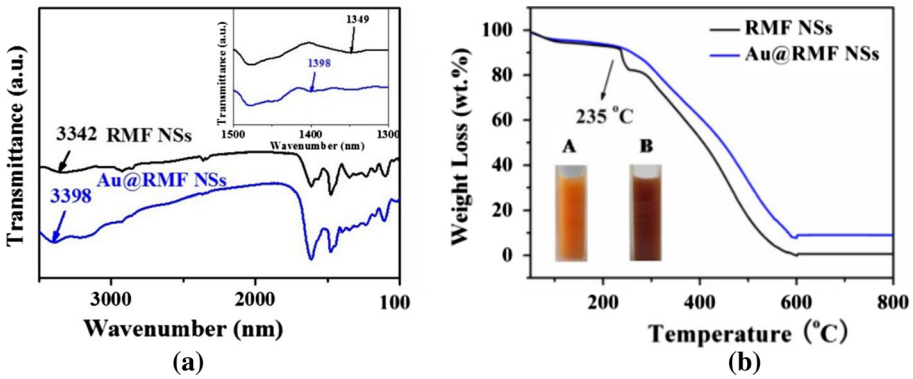

Fig. 4 Comparison for **a** FI-IR spectra (the *inset* shows the spectra between 1500 and 1300 nm) and **b** TGA curves of RMF NSs and Au@RMF NSs. *Inset* of **b** shows the photographs of RMF NSs **a** and Au@RMF NSs **b** dispersed in water after 2 weeks

remaining weight increased after loading Au NPs. Especially, it could be clearly seen that the decomposition of Au@RMF NPs composites is slower than that of RMF NSs at the range of 235–600 °C, which might be attributed to the interaction between Au NPs and RMF NSs [23]. The results also reveal that the Au@RMF NSs possess superior thermal stability to RMF NSs, which is important for the catalytic applications.

In addition, the RMF NSs exhibit a good solubility in polar solvents before and after modification with Au NPs, as shown in the inset of Fig. 4b. The color changes from red-brown (A) to wine-red (B) after the growth of Au NPs, conforming the uniform loading of Au NPs on RMS NSs. These nanospheres do not precipitate for 2 weeks for the reason that the OH^- groups owned by RMF NSs make it well soluble in polar solvent. High solubility of the nanostructures in water contributes to many applications in catalysis and bioelectrochemistry.

The as-prepared Au@RMF NSs were tested as catalyst for reduction of 4-NP reaction (Fig. 5) [41, 42]. In a typical experiment, the original absorption peak of fresh 4-NP was centered at 317 nm in neutral or acidic conditions and shifted to 400 nm immediately upon addition of prepared $NaBH_4$ solution, corresponding to a color change from light yellow to yellow green due to the formation of 4-nitrophenolate ions [43]. In absence of our catalysts, the adsorption peak at 400 nm, corresponding to the 4-nitrophenolate ions under alkaline conditions, remained unaltered even for 1 week. However, when a proper amount of Au@RMF NSs was present, we can clearly observe the immediate decolorization of the 4-NP solution (inset of Fig. 5a). After centrifugation, the supernatant was completely colorless, suggesting the end of the conversion. This is confirmed by the UV–vis absorbance vs. reaction time plots toward reductive of 4-NP reaction (Fig. 5a), which shows a gradual decrease of the 4-nitrophenolate ions peak at 400 nm with a simultaneous increase of the 4-AP peak at 295 nm with the isosbestic points at 319 and 276 nm. It is notable that the spectra have well-defined isosbestic points and this was an evident indication of sole product formation without any byproduct generation [44]. In this context, pseudo-first-order kinetics could be used to evaluate the kinetic reaction rate of the current catalytic reaction [45]. The kinetic rate constant k_{app} can be calculated from the rate equation $\ln(C_t/C_0) = -k_{app}t$, where C_0 is the initial concentration of 4-NP with a constant value of 2.0×10^{-4} mol L^{-1} and C_t represents the concentration of 4-NP at the time t. As shown in Fig. 5b, Au@RMF NSs exhibit a high activity with an estimated k_{app} value of 33×10^{-3} s^{-1}, superior to that of the present reported Au-based catalysts under ambient conditions [46–48]. The turnover frequency (TOF) means the number of moles of reduced 4-NP per mole of M atoms per second when the conversion has reached 90 % calculated [49]. The TOF of the Au@RMF NSs is estimated to be 279.2 s^{-1}, which is much better than other materials, such as Au@graphene oxide nanosheets (260 s^{-1}) [50] and Au@yolk-double shell SiO_2@Fe_3O_4/C microsphere (0.29 s^{-1}) [40].

To illustrate the superiority of our support, catalytic activities of different materials were further tested, Au-based NPs catalysts including Au@SiO_2 NSs and Au@active carbon hybrid materials (Fig. S3) were also synthesized by replacing the RMFs NSs with amino-group-modified SiO_2 NSs (diameter = 300 nm) and active carbon, respectively. As shown in Fig. 5c, the pure RMF NSs without Au NPs show no catalytic activity. Among these Au-based catalysts, Au@RMF NSs exhibit the highest activity ($k_{app} = 33 \times 10^{-3}$ s^{-1}), and their k_{app} is 11 times and 8.7 times higher than those of Au@SiO_2 NSs ($k_{app} = 3.0 \times 10^{-3}$ s^{-1}) and Au@active carbon ($k_{app} = 3.8 \times 10^{-3}$ s^{-1}). In addition to the Au-based catalysts, Ag NPs were also assembled on the RMFs and SiO_2 NSs, which were labeled as Ag@RMF NSs and Ag@SiO_2 NSs, respectively. Significantly, the Ag@RMFs NSs show a remarkably higher activity than Ag@SiO_2 NSs, suggesting a general excellent performance of RMF NSs for supporting metal NPs (Fig. 5d).

The stability of the catalyst should be taken into account in order to realize practical applications. As shown in

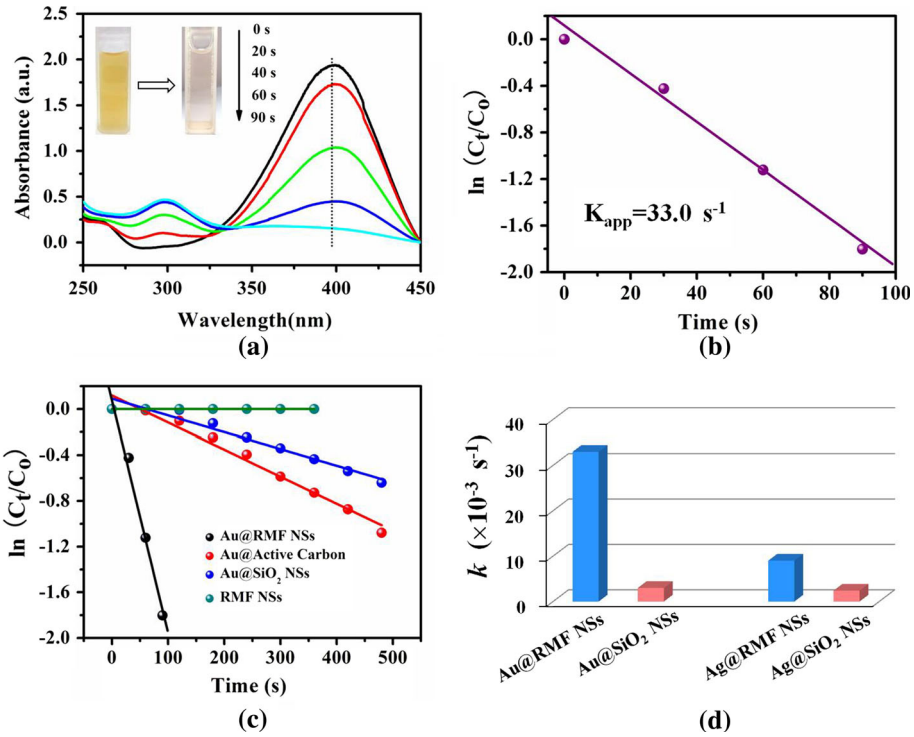

Fig. 5 **a** Successive UV–vis absorbance spectra for the reduction of 4-NP by $NaBH_4$ in the presence of Au@RMF NSs. **b** $\ln(C_t/C_0)$ *versus* reaction time (s) of Au@RMF NSs. **c** $\ln(C_t/C_0)$ *versus* reaction time (s) of Au@RMF NSs,Au@SiO_2 NSs, Au@active Carbon and RMF NSs and for comparison. **d** Kinetic rate constant (k) of Au@RMF NSs, Au@SiO_2 NSs, Ag@RMF NSs and Ag@SiO_2 NSs, respectively

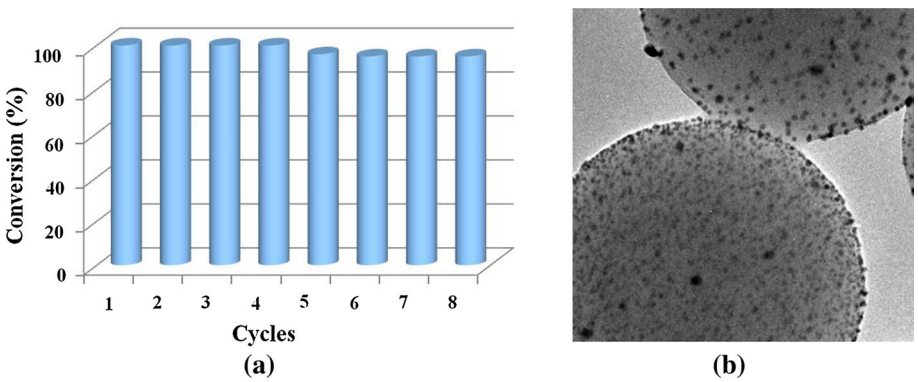

Fig. 6 **a** Conversion of 4-NP in eight successive cycles with Au@RMF NSs. **b** TEM image of Au@RMF NSs after eight reaction cycles

Fig. 6a, the conversion of 4-NP reaction over Au@RMF NSs catalyst remains as high as 93 % even after 8 successive cycles. Moreover, TEM analysis (Fig. 6a) of the Au@RMF NSs catalyst after recycle test reveals that the dispersion and size distribution of Au NPs do not show any obvious change compared with the fresh catalyst (Fig. 3b). To explore whether there is leaching during reactions, we performed a filtration to remove the Au@RMF NSs catalyst from the 4-NP solution when the reaction proceeded for 5 min. Next, the filtrate was continuatively stirred and monitored by UV–vis spectroscopy at regular intervals. It was found that the peak height at 400 nm remains nearly unchanged, suggesting that no leaching occurred.

The results from both the catalytic activity and stability studies indicate that the N-containing functionalities of the polymer supporter are an important role on the reduction of 4-NP catalysis enhancement in both the activity and stability of metal NPs. On the basis of these results, we suppose that such N-containing functionalities not only prevent metal NPs from movement and aggregation, but also is benefit for the preference capture of target molecules, allowing the increasing concentration of 4-NPs ions around the active metal NPs, which may be also an important for promoting the catalytic activity.

Although many works have demonstrated the adsorption of 4-NP ions on polymer substrates, few of them gave the precise simulation model toward reduction of 4-NP catalysis [51]. Herein, we investigated the adsorption model and the effect of the N-containing functionalities of polymer skeleton using DFT implemented in the

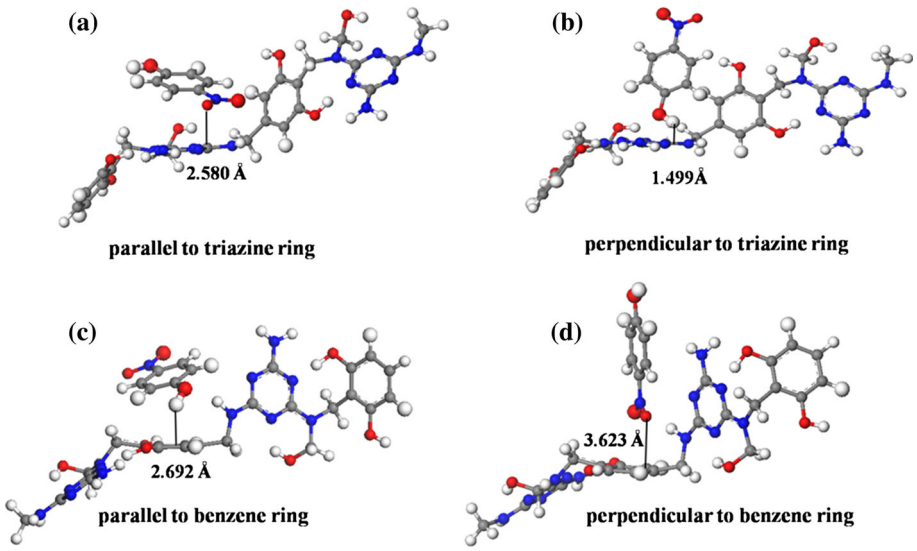

Fig. 7 The optimized structures of 4-NP ion adsorbed on RMF polymer: **a** parallel to triazine ring, **b** perpendicular to triazine ring, **c** parallel to benzene ring, and **d** perpendicular to benzene ring. The *gray*, *blue*, *red*, and *white* balls stand for C, N, O, and H atoms, respectively. The separated distances between 4-NP and triazine or benzene ring for each model have been marked correspondingly

Table 1 Energies and optimized distances of four different conformations

Conformations	Distance[a] (Å)	$E^{b}_{4\text{-NP}}$ (Ha)	E^{c}_{dimer} (Ha)	E^{d}_{system} (Ha)	E_{ads}(Ha)
Parallel to triazine ring	2.580	−512.009	−2041.092	−2553.112	−0.011
Perpendicular to triazine ring	1.499	−512.009	−2041.092	−2553.109	−0.008
Parallel to benzene ring	2.692	−512.009	−2041.092	−2533.053	20.048
Perpendicular to benzene ring	3.623	−512.009	−2041.092	−2533.070	20.032

[a] The distance is the most optimized between 4-NP and C_3N_3 ring or benzene ring

[b] $E_{4\text{-NP}}$ is energy of the isolated 4-NP ion

[c] E_{dimer} is energy of RMF dimer

[d] E_{system} is energy offree 4-NP ion on RMF dimer

Dmol3 code. In order to show a clear illustration, the optimized dimer structure of RMF molecular has been used to represent the microstructural information of the RMF polymer. Given that the RMF dimer consists of triazine- and benzene-rings, the computational simulation was performed based on four conformations: 4-NP ions adsorbed to the triazine- and benzene-rings from the parallel and perpendicular directions, respectively. As shown in Fig. 7, the 4-NP ion is closer to triazine-rings in both conformations, with the separated distances of 2.58 and 1.499 Å for parallel and perpendicular directions, respectively. Clearly, this results show the significantly superior adsorption behavior of 4-NP ions on triazine-rings than that for benzene-rings. Additionally, their adsorption energies calculated for 4-NP ions parallel and perpendicular to triazine-rings are −0.011 and −0.008 Ha, which is much stronger than that for parallel (20.048 Ha) and perpendicular (20.032 Ha) to benzene-rings, as listed on Table 1. The large separated distance coupled with weak adsorption energy of 4-NP ion on benzene indicates that it is not the preferred conformation. These are consistent with our experimental result, showing no catalytic effect for the RF resin NSs. The superior adsorption capacity of RMF NSs for 4-NP ions may be explained by the charge distributions. It is known that active site on triazine ring is positively charged due to the large electro-negativity of the N atoms. Consequently, the negatively charged free 4-NP ion is the preferred to adhere to the surface of RMF NSs.

Clearly, N-containing functional groups introduce unique opportunity to adsorption of 4-NP on the RMF NSs substrate, which is vital important to the following catalytic process. Our findings are fully agreement with the previous reports, showing that the doped N atoms in polymer and even graphene could introduce a great deal of positively charged active sites and high spin density to their adjacent atoms, leading to the preferred capture of the target organic molecules [25, 50, 52].

Conclusions

In conclusion, we have reported an advanced strategy for synthesis of well-defined N-containing polymer NSs (RMF NSs), which was employed as a functional platform for the dispersion of Au NPs, constructing the Au@RMF NSs hybrid nanostructures without any pre-modification. More importantly, the Au@RMF NSs exhibit the superior catalytic activity toward reduction of 4-NP reaction among the ever reported Au-based catalysts, and good recycle stability of conversion retention of 93 % even after eight reaction cycles. The adsorption model was established by computational simulation and was verified to be the significant step for the reduction of 4-NP catalysis. Accordingly, the N-containing functional groups of RMF NSs offer simultaneously immobilization site to prevent the active metal NPs from movement and aggregation and local preference capture site of target molecules, giving the increasing concentration of 4-NPs ions around the active metal NPs, which may be important for accelerating the catalytic kinetics. The experiment results coupled with computational calculation might open up a new avenue in the development of high-performance catalysts toward liquid, gas, and electrochemical reaction.

Acknowledgements This work was financially supported by the National Natural Science Foundation of China (Nos. 21101141 and 51202223), Program for New Century Excellent Talents in Universities (NCET), the Open Project Foundation of State Key Laboratory of Inorganic Synthesis and Preparation Chemistry of Jilin University (2012-13).

References

1. Chiou JR, Lai BH, Hsu KC, Chen DH (2013) One-Pot Green synthesis of silver/iron oxide composite nanoparticles for 4-nitrophenol reduction. J Hazard Mater 248:394–400
2. Corma A, Serna P, Concepcion P, Calvino JJ (2008) Transforming nonselective into chemoselective metal catalysts for the hydrogenation of substituted nitroaromatics. J Am Chem Soc 130:8748–8753
3. Wunder S, Polzer FL, Mei Y, Ballauff YM (2010) Kinetic analysis of catalytic reduction of 4-nitrophenol by metallic nanoparticles immobilized in spherical polyelectrolyte brushes. J Phys Chem C 114:8814–8820
4. Zhang YW, Liu S, Lu WB, Wang L, Tian JQ, Sun XP (2011) In situ green synthesis of Au nanostructures on graphene oxide and their application for catalytic reduction of 4-Nitrophenol. Catal Sci Technol 1:1142–1144
5. Yuan CH, Luo WA, Zhong LN, Deng HJ, Liu J, Xu YT, Dai LZ (2011) Gold@polymer nanostructures with tunable permeability shells for selective catalysis. Angew Chem Int Ed 50:3515–3519
6. Lv WP, Wang Y, Feng WQ, Qi JJ, Zhang GL, Zhang FB, Fan XB (2011) Robust and smart gold nanoparticles: one-step synthesis, tunable optical property, and switchable catalytic activity. J Mater Chem 21:6173–6178
7. Sawada KC, Sakai SJ, Taya MS (2014) Polyacrylonitrile-based electrospun nanofibers carrying gold nanoparticles in situ formed by photochemical assembly. J Mater Sci 49:4595–46008. doi:10.1007/s10853-014-8161-z
8. Zhang CX, Li C, Chen YY, Zhang Y (2014) Synthesis and catalysis of Ag nanoparticles trapped into temperature-sensitive and conductive polymers. J Mater Sci 49:6872–6882. doi:10.1007/s10853-014-8389-7
9. Wang XX, Ji HF, Zhang X, Zhang H, Yang XL (2010) Hollow polymer microspheres containing a gold nanocolloid core adsorbed on the inner surface as a catalytic microreactor. J Mater Sci 45:3981–3989. doi:10.1007/s10853-010-4470-z
10. Yan W, Chen B, Mahurin SM, Dai S, Overbury SH (2004) Brookite-supported highly stable gold catalytic system for CO oxidation. Chem Commun 17:1918–1919
11. Ma Z, Liang C, Overbury S, Dai S (2007) Gold nanoparticles on electroless-deposition-derived MnOx/C: synthesis, characterization, and catalytic CO oxidation. J Catal 252:119–126
12. Ma Z, Overbury SH, Dai S (2007) Au/MxOy/TiO_2 catalysts for CO oxidation: promotional effect of main-group, transition, and rare-earth metal oxide additives. J Mol Catal A: Chem 273:186–197
13. Zhang LF, Aboagye A, Kelkar A, Lai CL, Fong H (2014) A review: carbon nanofibers from electrospun polyacrylonitrile and their applications. J Mater Sci 49:463–480. doi:10.1007/s10853-013-7705-y
14. Fang Y, Wang E (2013) Simple and direct synthesis of oxygenous carbon supported palladium nanoparticles with high catalytic activity. Nanoscale 5:1843–1848
15. Liang M, Su RX, Qi W, Yu YJ, Wang LB, He ZM (2014) Synthesis of well-dispersed Ag nanoparticles on eggshell membrane for catalytic reduction of 4-nitrophenol. J Mater Sci 49:1639–1647. doi:10.1007/s10853-013-7847-y
16. Shan J, Tenhu H (2007) Recent advances in polymer protected gold nanoparticles: synthesis, properties and applications. Chem Commun 44:4580–4598
17. Liu X, Cheng F, Liu Y, Liu HJ, Chen Y (2010) Preparation and characterization of novel thermoresponsive gold nanoparticles and their responsive catalysis properties. J Mater Chem 20:360–368
18. Seo E, Kim J, Hong Y, Kim YS, Lee D, Kim BS (2013) Double hydrophilic block copolymer templated Au nanoparticles with enhanced catalytic activity toward nitroarene reduction. J Phys Chem C 117:11686–11693
19. Wang ML, Jiang TT, Lu Y, Liu HJ, Chen Y (2013) Gold nanoparticles immobilized in hyperbranched polyethylenimine modified polyacrylonitrile fiber as highly efficient and recyclable heterogeneous catalysts for the reduction of 4-nitrophenol. J Mater Chem A 1:5923–5933
20. Wang X, Fu J, Wang M, Wang Y, Chen Z, Zhang J, Chen J, Xu Q (2014) Facile synthesis of au nanoparticles supported on polyphosphazene functionalized carbon nanotubes for catalytic reduction of 4-nitrophenol. J Mater Sci 49:5056–5065. doi:10.1007/s10853-014-8212-5
21. Wu S, Dzubiella J, Kaiser J, Drechsler M, Guo X, Ballauff M, Lu Y (2012) Thermosensitive Au-PNIPA yolk-shell nanoparticles with tunable selectivity for catalysis. Angew Chem Int Ed 51:2229–2233
22. Zhang J, Chen G, Chaker M, Rosei F, Ma D (2013) Gold nanoparticle decorated ceria nanotubes with significantly high catalytic activity for the reduction of nitrophenol and mechanism study. Appl Catal B-Environ 132–133:107–115
23. Zhang P, Shao C, Zhang Z, Zhang M, Mu J, Guo Z, Liu Y (2011) In Situ assembly of well-dispersed Ag Nanoparticles (Ag NPs) on electrospun carbon nanofibers (CNFs) for catalytic reduction of 4-nitrophenol. Nanoscale 3:3357–3363

24. Su F, Tian Z, Poh CK, Wang Z, Lim SH, Liu Z, Lin J (2010) Pt nanoparticles supported on nitrogen-doped porous carbon nanospheres as an electrocatalyst for fuel cells. Chem Mater 22:832–839
25. Kong XK, Sun ZY, Chen M, Chen CL, Chen QW (2013) Metal-free catalytic reduction of 4-nitrophenol to 4-aminophenol by N-doped graphene. Energy Environ Sci 6:3260–3266
26. Liang J, Du X, Gibson C, Du XW, Qiao SZ (2013) N-Doped graphene natively grown on hierarchical ordered porous carbon for enhanced oxygen reduction. Adv Mater 25:6226–6231
27. Yoon H, Ko S, Jang J (2007) Nitrogen-doped magnetic carbon nanoparticles as catalyst supports for efficient recovery and recycling. Chem Commun 14:1468–1470
28. Xie X, Long J, Xu J, Chen L, Wang Y, Zhang Z, Wang X (2012) Nitrogen-doped graphene stabilized gold nanoparticles for aerobic selective oxidation of benzylic alcohols. RSC Adv 2:12438
29. Guo S, Zhai J, Fang Y, Dong S, Wang E (2008) Nanoelectrocatalyst based on high-density Au/Pt Hybrid nanoparticles supported on a silica nanosphere. Chem Asian J 3:1156–1162
30. Hohenberg P, Kohn W (1964) Inhomogeneous electron gas. Phys Rev 14:B864–B871
31. Perdew JP, Wang Y (1991) Phys Rev B 334:13244
32. Zhang J, Guo S, Wei J, Xu Q, Yan W, Fu J, Wang S, Cao M, Chen Z (2013) High-efficiency encapsulation of Pt nanoparticles into the channel of carbon nanotubes as an enhanced electrocatalyst for methanol oxidation. Chem Eur J 19:16087–16092
33. Mohamed MM, Al Sharif MS (2013) Visible light assisted reduction of 4-nitrophenol to 4-aminophenol on Ag/TiO_2 photocatalysts synthesized by hybrid templates. Appl Catal B 142: 432–441
34. Ma FW, Zhao H, Sun LP, Li Q, Huo LH, Xia T, Gao S, Pang GS, Shi Z, Feng SH (2012) A facile route for nitrogen-doped hollow graphitic carbon spheres with superior performance in supercapacitors. J Mater Chem 22:13464–13468
35. Zhou HH, Xu S, Su HP, Wang M, Qiao WM, Ling LC, Long DH (2013) Facile preparation and ultra-microporous structure of melamine–resorcinol–formaldehyde polymeric microspheres. Chem Commun 49:3763–3765
36. Park KY, Jang JH, Hong JE, Kwon YU (2012) Mesoporous thin films of nitrogen-doped carbon with electrocatalytic properties. J Phys Chem C 116:16848–16853
37. Lee WH, Lee JG, Reucroft PJ (2001) XPS study of carbon fiber surfaces treated by thermal oxidation in a gas mixture of O_2/($O_2 + N_2$). Appl Surf Sci 171:136–142
38. Lin H, Kai T, Hua DY, Ma Z, Zhou SH (2013) Size effect of gold nanoparticles in catalytic reduction of p-nitrophenol with $NaBH_4$. Molecules 18:12609–12620
39. Fu JW, Wang MH, Zhang C, Xu Q, Huang XB, Tang XZ (2011) Controlled fabrication of noble metal nanoparticles loaded on the surfaces of cyclotriphosphazene-containing polymer nanotubes. J Mater Sci 47:1985–1991. doi:10.1007/s10853-011-5994-6
40. Zeng T, Zhang XL, Wang SH, Ma YR, Niu HY, Cai YQ (2013) A double-shelled yolk-like structure as an ideal magnetic support of tiny gold nanoparticles for nitrophenol reduction. J Mater Chem A 1:11641–11647
41. Tang SC, Vongehr S, Meng XK (2010) Controllable incorporation of Ag and Ag–Au nanoparticles in carbon spheres for tunable optical and catalytic properties. J Mater Chem 20:5436–5445
42. Zhang ZY, Shao CL, Sun YY, Mu JB, Zhang MY, Zhang P, Guo ZC, Liang PP, Wang CH, Liu YC (2012) Tubular nanocomposite catalysts based on size-controlled and highly dispersed silver nanoparticles assembled on electrospun silica nanotubes for catalytic reduction of 4-nitrophenol. J Mater Chem 22:1387–1395
43. Tian J, Liu GN, Guan C, Zhao HY (2013) Amphiphilic gold nanoparticles formed at a liquid-liquid interface and fabrication of hybrid nanocapsules based on interfacial uv photodimerization. Polym Chem 4:1913–1920
44. Shin HS, Huh S (2012) Au/Au@polythiophene core/shell nanospheres for heterogeneous catalysis of nitroarenes. ACS Appl Mater Interfaces 4:6324–6331
45. Jiang HL, Akita T, Ishida T, Haruta M, Xu Q (2011) Synergistic catalysis of Au@Ag core-shell nanoparticles stabilized on metal-organic framework. J Am Chem Soc 133:1304–1306
46. Li J, Liu CY, Liu Y (2012) Au/graphene hydrogel: synthesis, characterization and its use for catalytic reduction of 4-nitrophenol. J Mater Chem 22:8426–8430
47. Guan BY, Wang X, Xiao Y, Liu YL, Huo QS (2013) A versatile cooperative template-directed coating method to construct uniform microporous carbon shells for multifunctional core-shell nanocomposites. Nanoscale 5:2469–2475
48. Agrawal G, Schürings MP, Van Rijn P, Pich A (2013) Formation of catalytically active gold-polymer microgel hybrids via a controlled in situ reductive process. J Mater Chem A 1:13244–13251
49. Vix Guterl C, Frackowiak E, Jurewicz K, Friebe M, Parmentier J, Béguin F (2005) Electrochemical energy storage in ordered porous carbon materials. Carbon 43:1293–1302
50. Choi Y, Bae HS, Seo E, Jang S, Park KH, Kim BS (2011) Hybrid gold nanoparticle-reduced graphene oxide nanosheets as active catalysts for highly efficient reduction of nitroarenes. J Mater Chem 21:15431–15436
51. Lu Y, Mei Y, Schrinner M, Ballauff M, Moller MW, Breu J (2007) In situ formation of Ag nanoparticles in spherical polyacrylic acid brushes by UV irradiation. J Phys Chem C 111: 7676–7681
52. Amirfakhri SJ, Binny D, Meunier JL, Berk D (2014) Investigation of hydrogen peroxide reduction reaction on graphene and nitrogen doped graphene nanoflakes in neutral solution. J Power Sources 257:356–363